Electronic Supplementary Information

for

Peptide Interdigitation-Induced Twisted Nanoribbons as Chiral Scaffolds for Supramolecular Nanozymes

Shuxin Song,[a] Jingyu Wang,[b] Na Song,[a] Huixia Di,[c] Dingbin Liu,[c] and Zhilin Yu[a]*

[a] Key Laboratory of Functional Polymer Materials, Ministry of Education
State Key Laboratory of Medicinal Chemical Biology
Institute of Polymer Chemistry, College of Chemistry, Nankai University, Tianjin 300071, China

[b] School of Biomedical Engineering and Technology
Tianjin Medical University, Tianjin 300070, China

[c] College of Chemistry, Research Center for Analytical Sciences, State Key Laboratory of Medicinal Chemical Biology, and Tianjin Key Laboratory of Molecular Recognition and Biosensing, Nankai University, Tianjin 300071, China

1. General Materials

All Fmoc-protected amino acids, Rink amide 4-methyl-benzhydrylamine (MBHA) resin (Loading density: 0.51 mmol/g) and hexafluorophosphate azabenzotriazole tetramethyl uronium (HATU) used in solid-phase peptide synthesis were obtained from Bide Pharmatech Co., Ltd. (China). Palmitoyl chloride and 12-amino dodecanoic acid were purchased from TCI (China). Organic solvents including N, N′-dimethylformamide (DMF), dichloromethane (CH_2Cl_2), methanol (CH_3OH), acetonitrile (CH_3CN), N, N′-diisopropylethylamine (DIEA), and trifluoroacetic acid (TFA) were purchased from Tianjin Concord Technology Co., Ltd (China). Piperidine and triisopropylsilane were obtained from Sinopharm Chemical Reagent Co., Ltd. (China) and Meryer Chemical Technology Co. Ltd. (China), respectively. Thioflavin T (Th-T), chloroauric acid ($HAuCl_4$), sodium citrate, sodium borohydride ($NaBH_4$) and Hydrogen peroxide (H_2O_2) was obtained from J&K Scientific Ltd. (China). D- and L-3,4-dihyroxy-phenylalanine (DOPA) were purchased from Energy Chemical Reagent Co., Ltd. (China). 3,3′,5,5′-Tetramethylbenzidine (TMB) was purchased from Heowns Co., Ltd. (China). Water used in all experiments was purified by Arium Pro Ultrapure water systems (Sartorius, 18.2 MΩ).

2. Purification of LIPIAs 1-6 and Ac-LIPIA 1

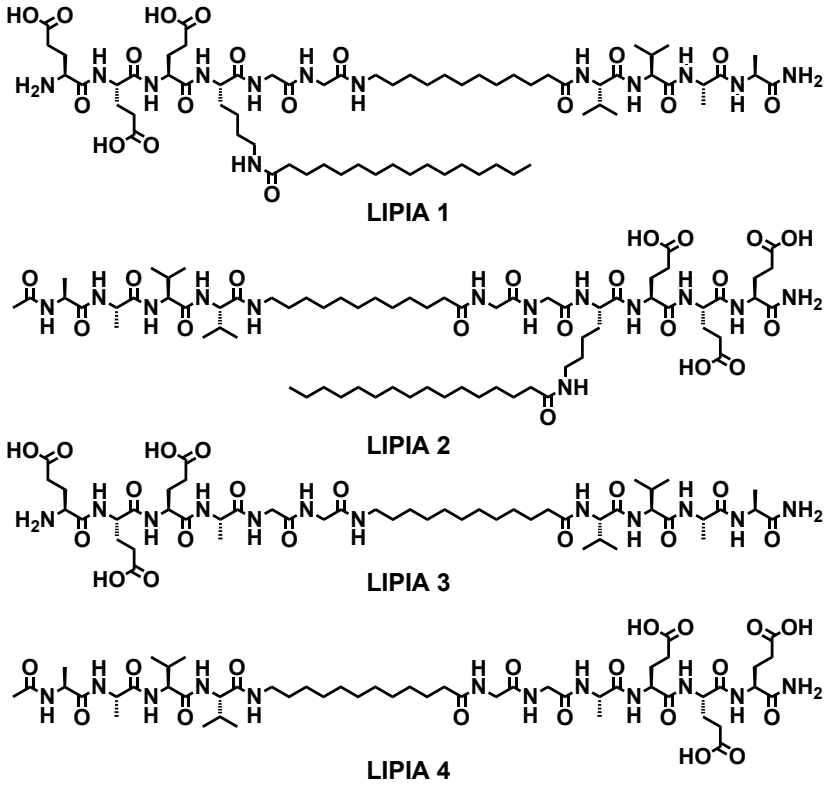

Figure S1. Chemical structures of LIPIAs **1-4**.

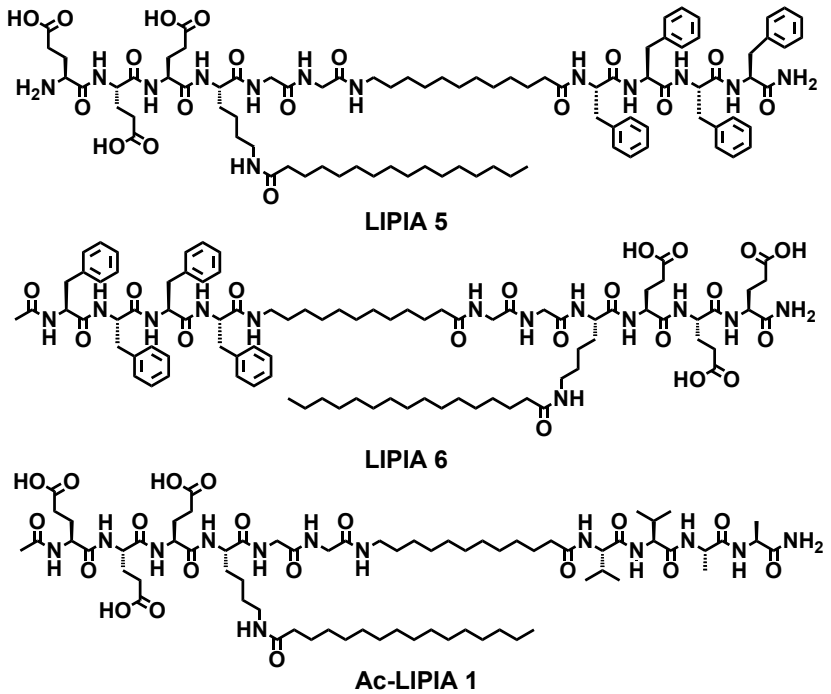

Figure S2. Chemical structures of LIPIAs **5** and **6**, as well as Ac-LIPIA **1**.

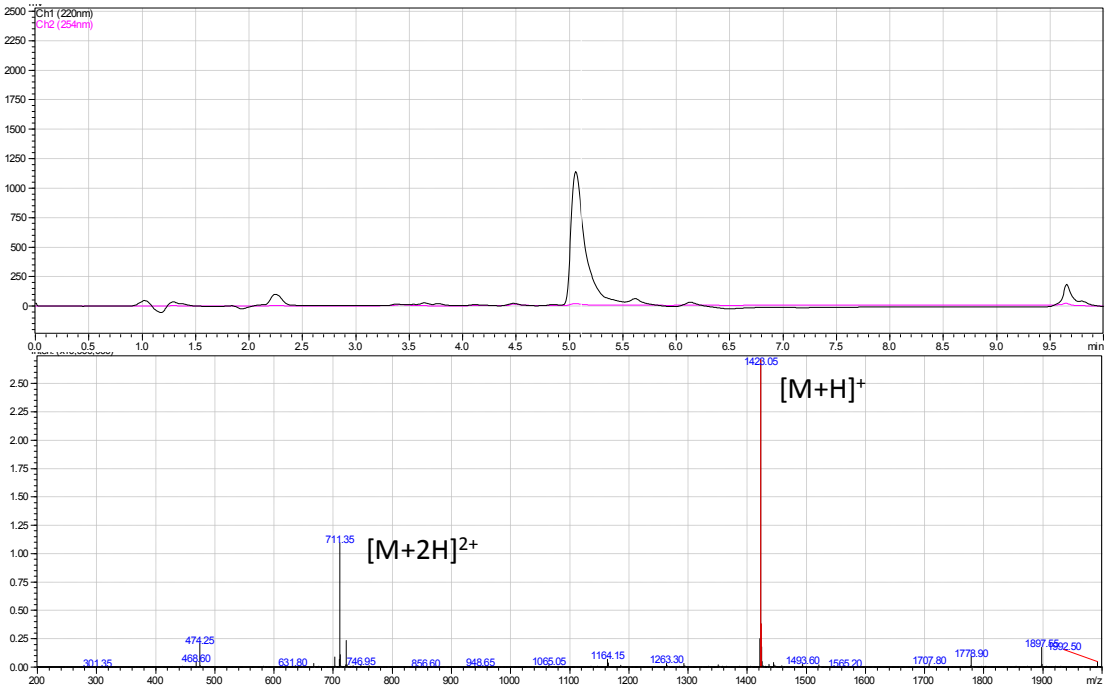

Figure S3. LC trace (top, black and pink lines monitored at 224 and 254 nm, respectively) and MS spectrum (bottom) of LIPIA **1**.

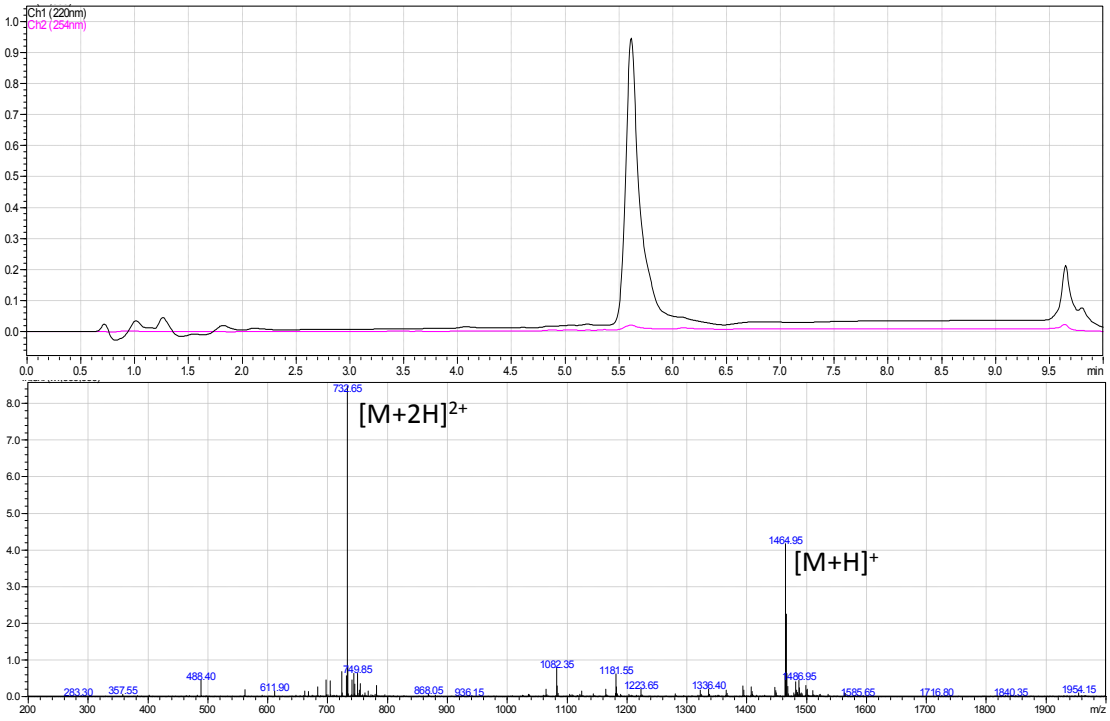

Figure S4. LC trace (top, black and pink lines monitored at 224 and 254 nm, respectively) and MS spectrum (bottom) of LIPIA **2**.

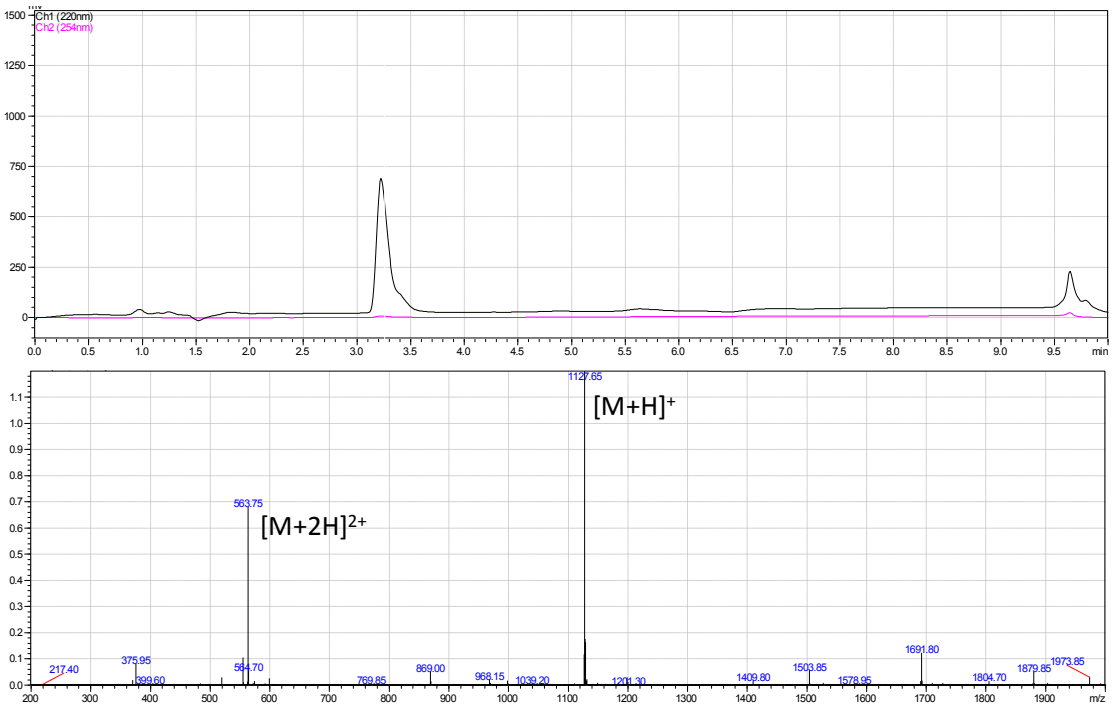

Figure S5. LC trace (top, black and pink lines monitored at 224 and 254 nm, respectively) and MS spectrum (bottom) of LIPIA **3**.

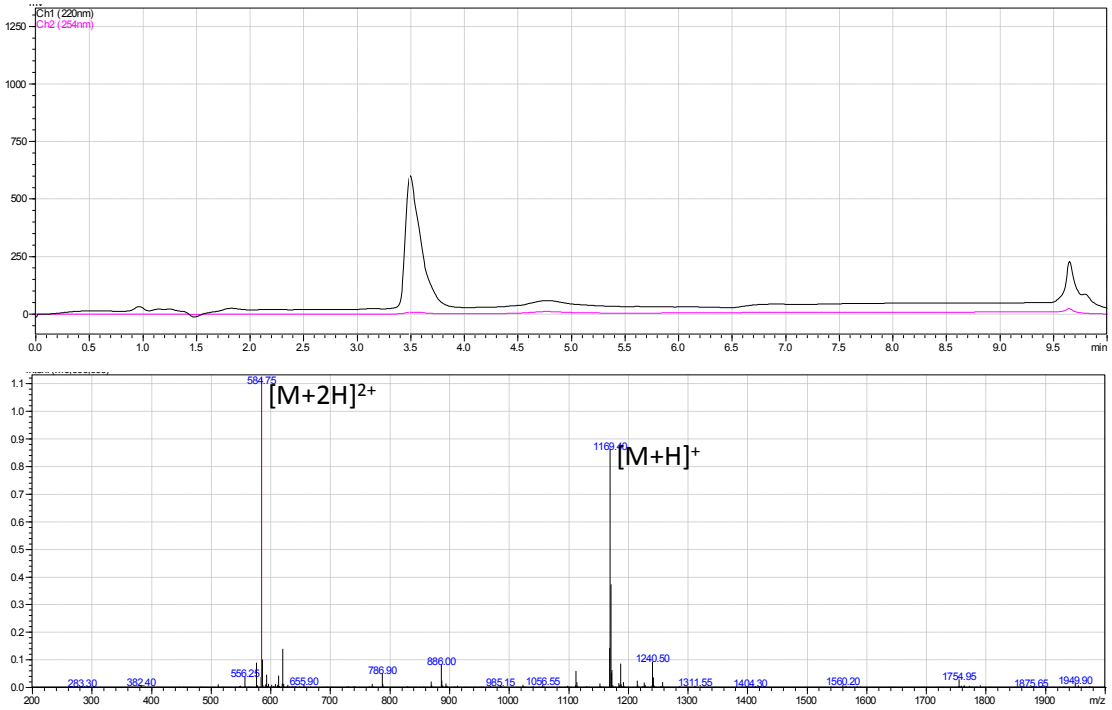

Figure S6. LC trace (top, black and pink lines monitored at 224 and 254 nm, respectively) and MS spectrum (bottom) of LIPIA **4**.

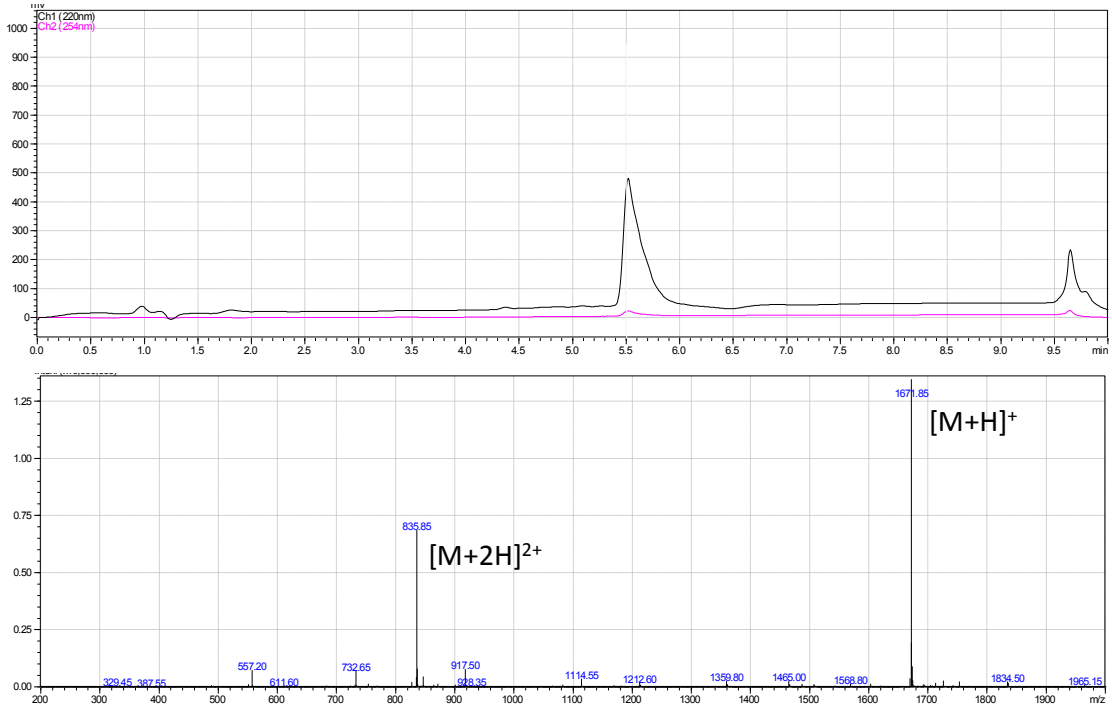

Figure S7. LC trace (top, black and pink lines monitored @ 224 and 254 nm, respectively) and MS spectrum (bottom) of LIPIA **5**.

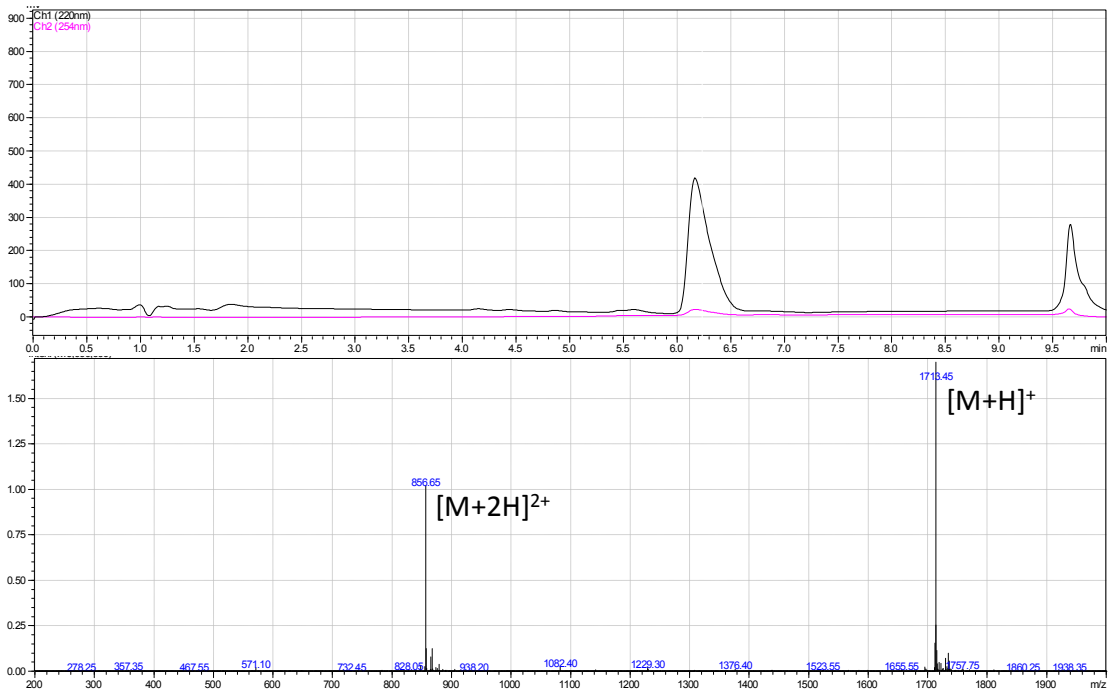

Figure S8. LC trace (top, black and pink lines monitored @ 224 and 254 nm, respectively) and MS spectrum (bottom) of LIPIA **6**.

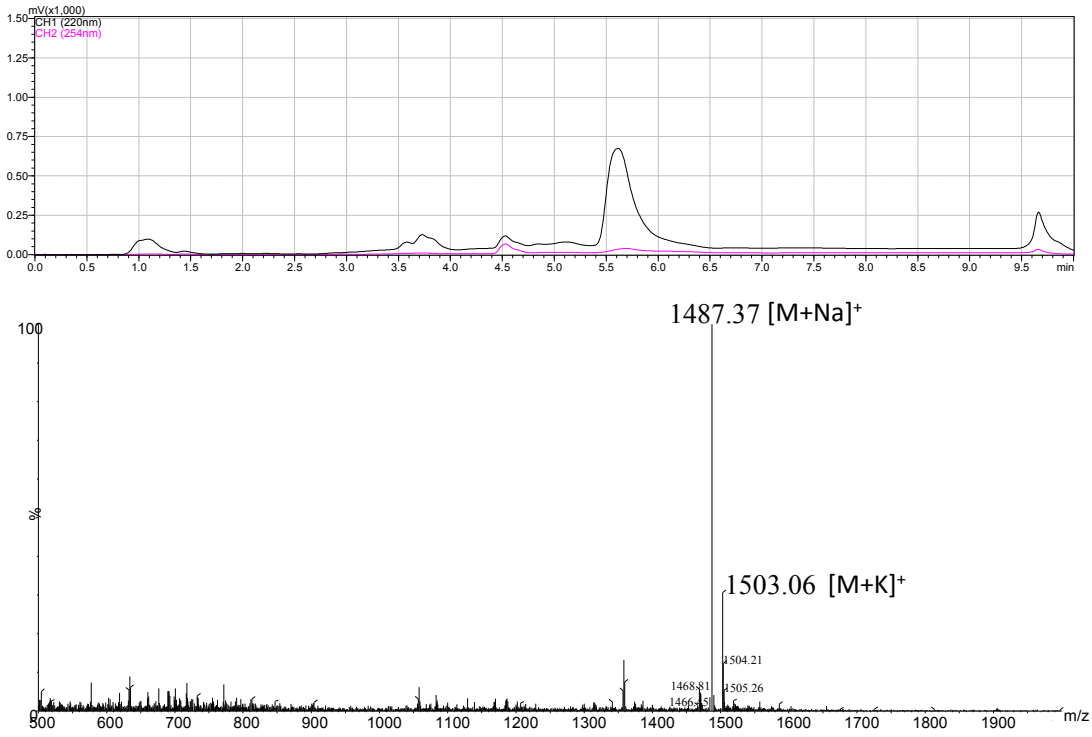

Figure S9. LC trace (top, black and pink lines monitored @ 224 and 254 nm, respectively) and MS spectrum (bottom) of Ac-LIPIA **1**.

3. Conformation and Morphology Characterizations

^{19}F NMR Spectra

The ^{19}F NMR spectrum was recorded on a Varian 400 MHz spectrometer at room temperature.

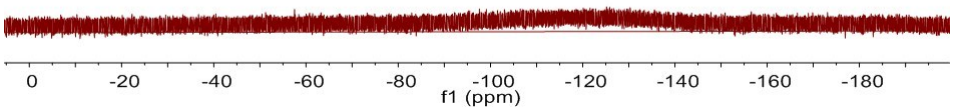

Figure S10. ^{19}F NMR spectra of LIPIA **1** (2 mM, D_2O) at room temperature.

To confirm the relationship between the FTIR absorbance signals and the secondary structures of LIPIA **1**, we carried out the ^{19}F NMR study to identify the FTIR signals

in the range of 1650-1680 cm^{-1}. ^{19}F NMR spectrum of LIPIA **1** did not show obvious ^{19}F NMR signals, indicating the absence of TFA salts in LIPIA **1**. Therefore the FTIR signals in the range of 1660-1690 cm^{-1} are associated with the antiparallel β-sheets formed by LIPIA **1**.

Circular Dichroism (CD) Spectroscopy

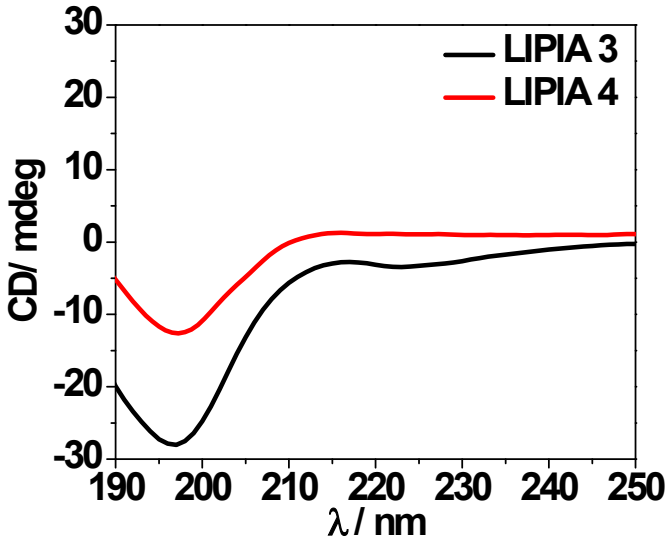

Figure S11. CD spectra of LIPIAs **3** and **4**.

CD spectra displayed a remarkable negative band at approximately 197 nm for LIPIA **3** and **4**, respectively. These results suggest the random coil conformation for LIPIAs **3** and **4** in solution, in contrast to the β-sheets formed by LIPIAs **1** and **2**. This finding indicates the significant role of the two-tailed motifs and the hydrophobic interactions among the side palmityl tail in the peptide-interdigitating mechanism for the formation of β-sheets by LIPIAs.

Thioflavin T (ThT) Binding Assay

Thioflavin T (ThT) binding assays were performed in quartz cuvettes with a total volume of 2 mL. The LIPIA solutions (200 μM, 1.6 mL) were incubated with ThT (100 μM, 400 μL) overnight before measurement. Fluorescence spectra were recorded by an Agilent Cary Eclipse fluorescence spectrophotometer with an excitation and emission slit width of 1.5 nm and 20 nm, respectively.

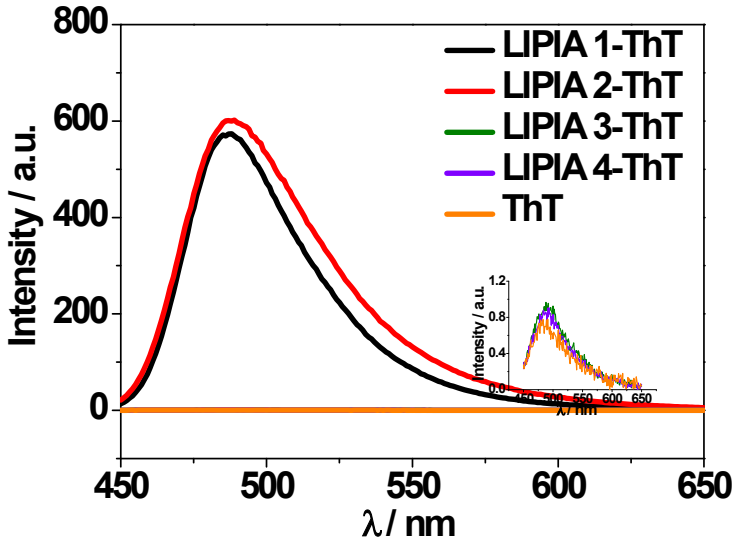

Figure S12. Fluorescence spectra of the solutions of ThT molecule alone or in the presence of LIPIAs **1**, **2**, **3**, and **4** excited at 421 nm. The inset panel showed the spectra of ThT alone or in the presence of LIPIA **3** and **4**, due to the extremely low fluorescence intensity.

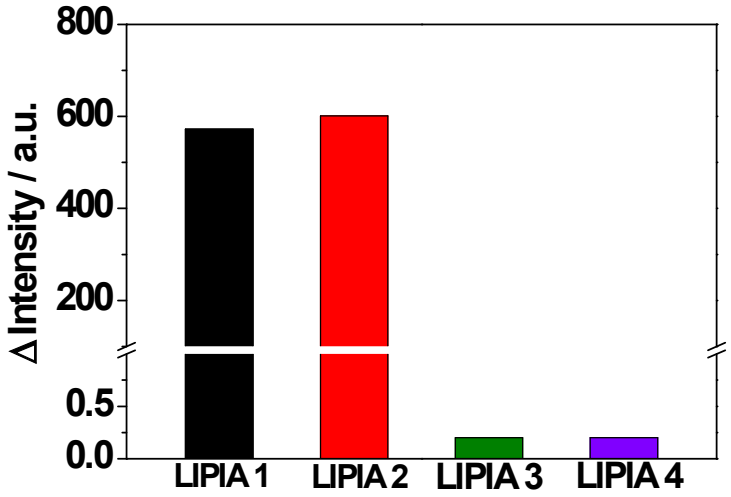

Figure S13. The normalized maximal emission intensity of ThT solutions in the presence of LIPIAs **1**, **2**, **3**, and **4** compared to ThT molecules alone.

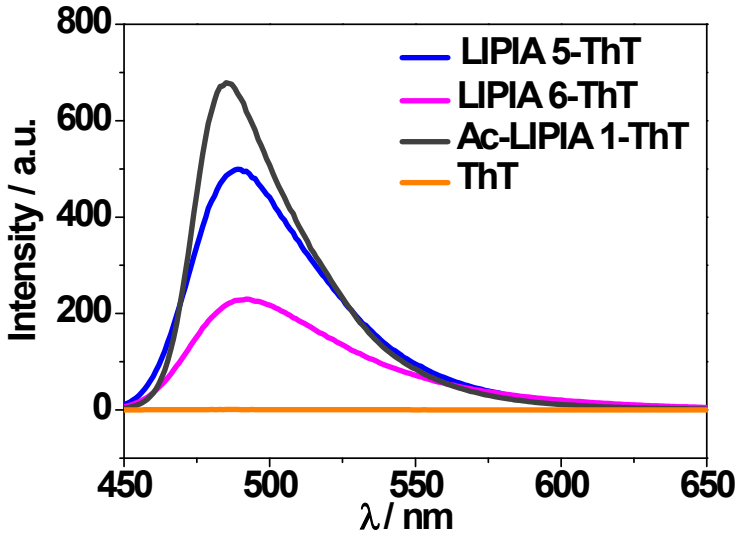

Figure S14. Fluorescence spectra of the solutions of ThT molecules alone or in the presence of LIPIAs **5**, **6**, and Ac-LIPIA **1** excited at 421 nm.

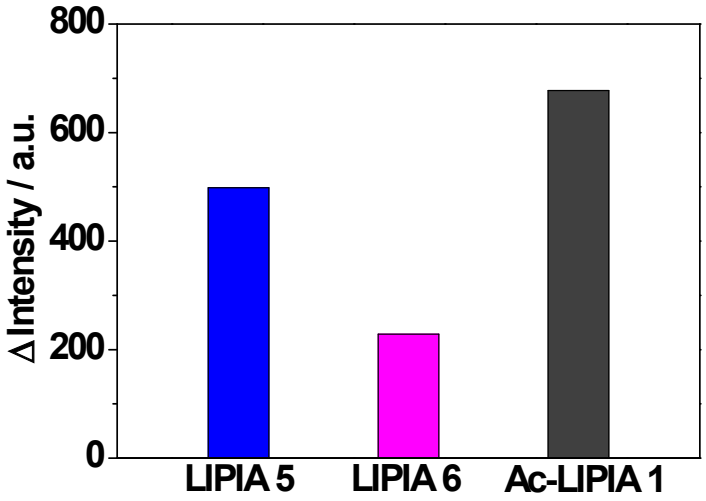

Figure S15. The normalized maximal emission intensity of ThT solutions in the presence of LIPIAs **5**, **6**, and Ac-LIPIA **1** compared to ThT molecules alone.

Critical Aggregation Concentration (CAC)

The CAC values of LIPIAs **1** and **2** were estimated by using Nile Red as the fluorescent probe based on the emission shift of Nile Red associated with its microenvironment.[1] The LIPIA solutions (2 mL) with different concentrations were prepared by diluting the annealed solutions (2 mM) into small vials. Subsequently, 2 μL of the stock solution of Nile Red (100 μM) in ethanol was added to each vial, leading to a concentration of 100 nM for Nile Red in the LIPIA samples. The LIPIA samples containing Nile Red were aged overnight before measurement. Fluorescence spectra were recorded on an Agilent Cary Eclipse fluorescence spectrophotometer with an excitation wavelength of 550 nm. Plotting the wavelength of the maximal emission of Nile Red as a function of the concentration of LIPIAs results in the curves for estimation of CAC values.

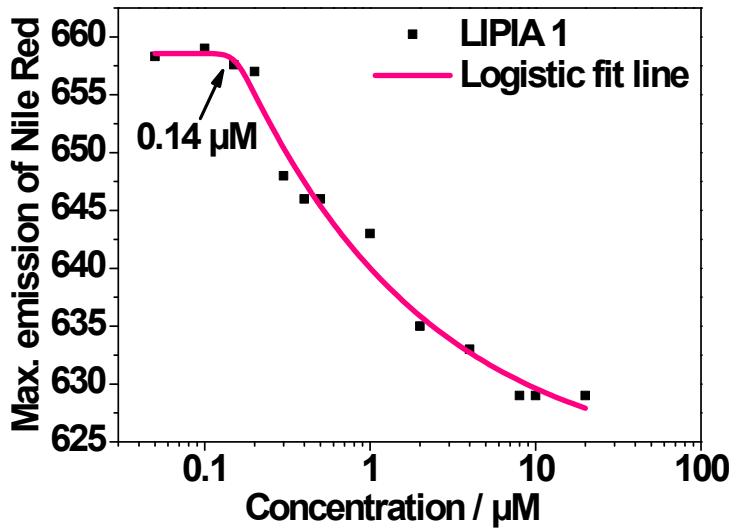

Figure S16. The wavelengths of the maximal emission of Nile Red in the presence of LIPIA **1** as a function of the concentration of LIPIA **1** in the range of 0.05 and 20 µM.

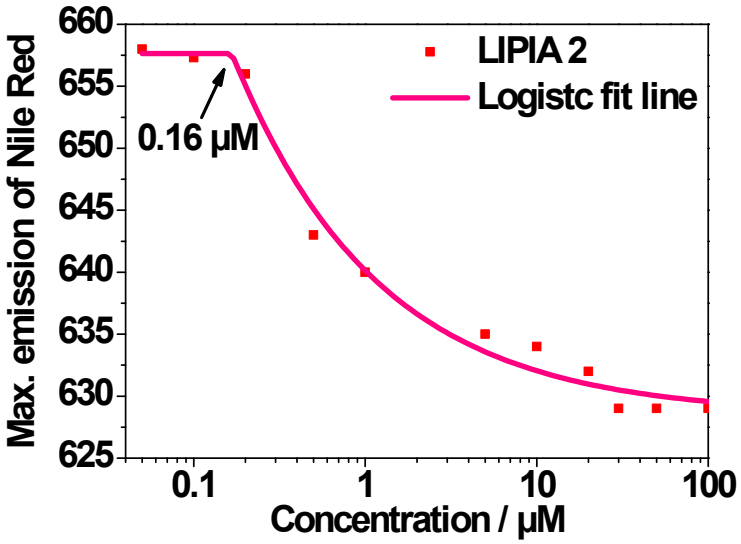

Figure S17. The wavelengths of the maximal emission of Nile Red in the presence of LIPIA **2** as a function of the concentration of LIPIA **2** in the range of 0.05 and 100 µM. Monitoring the shift of the wavelength of the maximal emission of Nile Red allows us to estimate that LIPIAs **1** and **2** start to aggregate below the concentration of 0.2 µM, thus demonstrating the remarkable propensity of LIPIAs **1** and **2** to assemble in aqueous medium.

Atomic Force Microscopic Images (AFM)

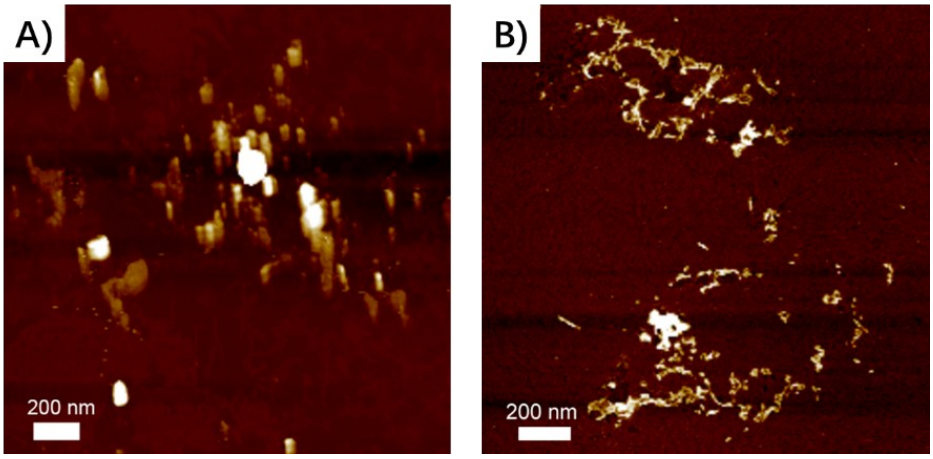

Figure S18. AFM images of the aggregates formed by LIPIAs **3** (A) and **4** (B), in which no regular ordered nanostructures were observed.

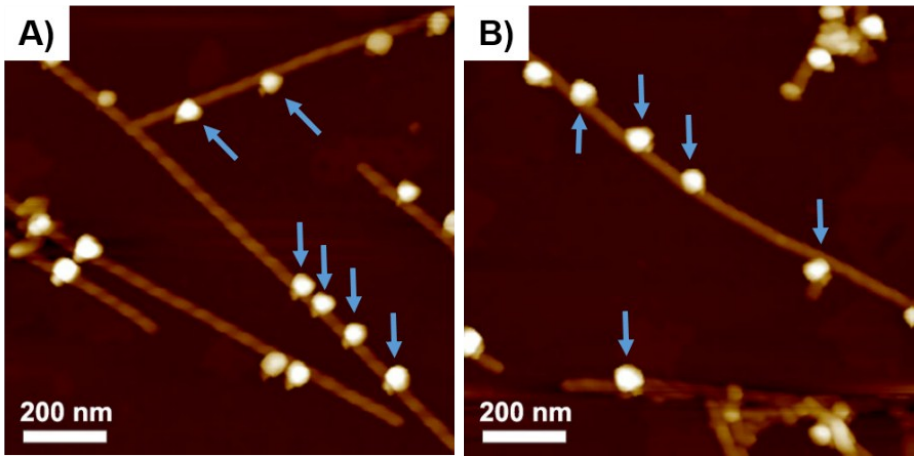

Figure S19. AFM images of AuNP@LIPIA **1** (A) and AuNP@LIPIA **2** (B), in which the blue arrows indicate the captured gold nanoparticles on the twisted or flat nanoribbons formed by LIPIAs **1** and **2**, respectively.

Transmission Electron Microscopic Images (TEM)

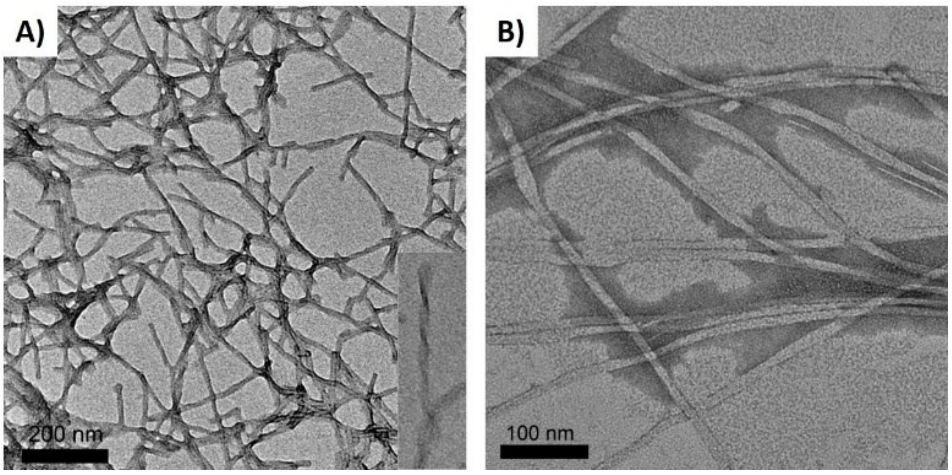

Figure S20. TEM images of LIPIAs **5** (A) and **6** (B).

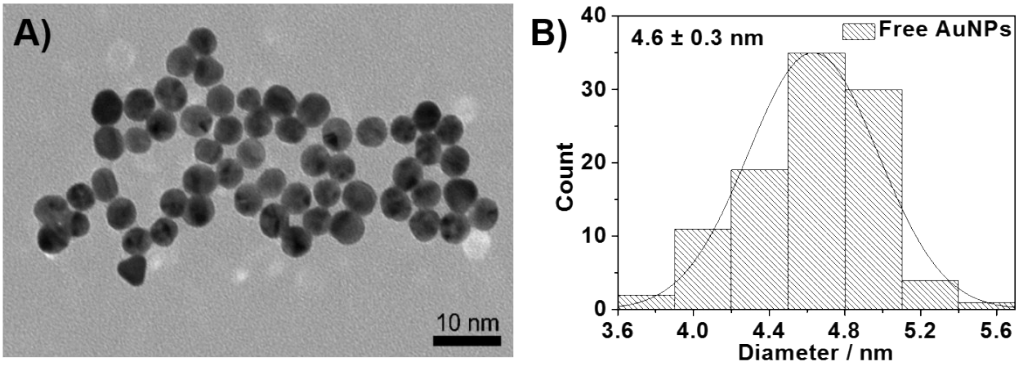

Figure S21. TEM image and the distribution of the diameter of free gold nanoparticles.

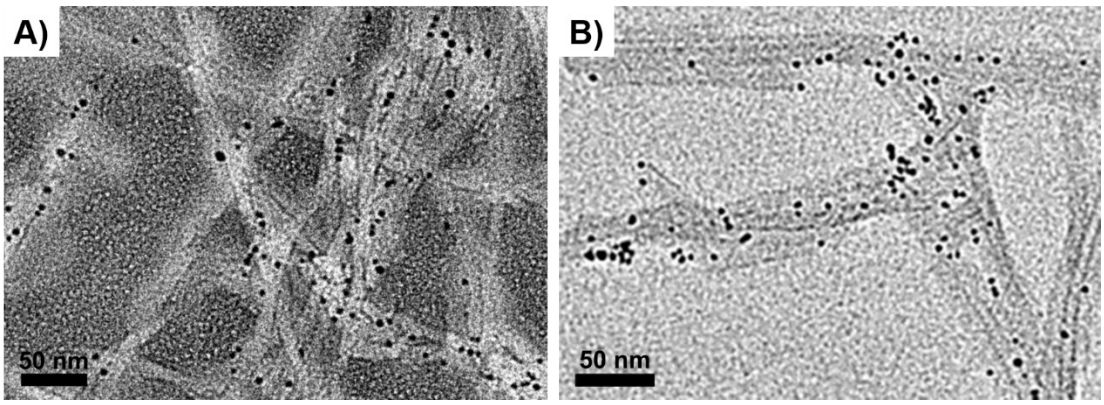

Figure S22. Magnified TEM images of AuNP@LIPIA **1** (A) and AuNP@LIPIA **2** (B).

4. Molecular Models of LIPIA Dimers

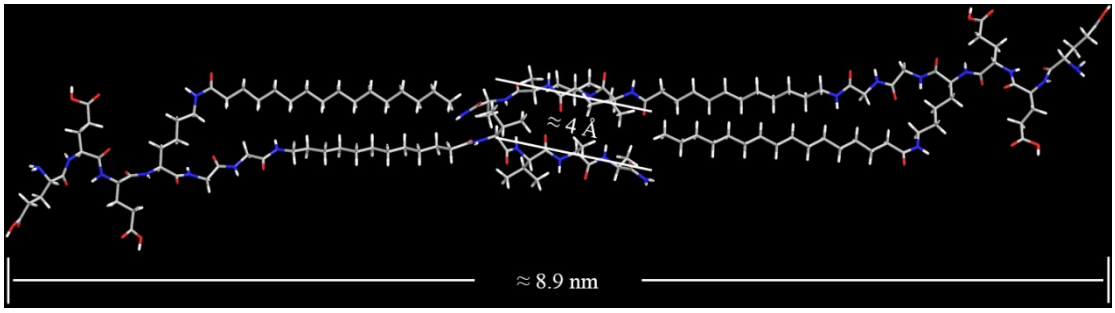

Figure S23. Molecular model of the dimer of LIPIA **1** obtained by a MM2 energy minimization calculation.

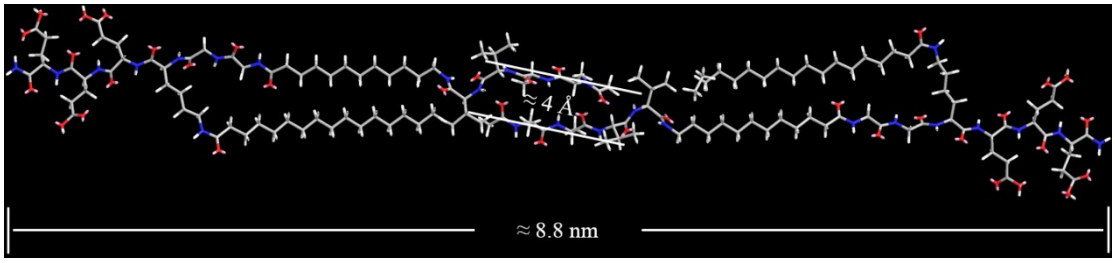

Figure S24. Molecular model of the dimer of LIPIA **2** obtained by a MM2 energy minimization calculation.

5. Preparation of Supramolecular Nanozymes AuNP@LIPIA 1 and AuNP@LIPIA 2

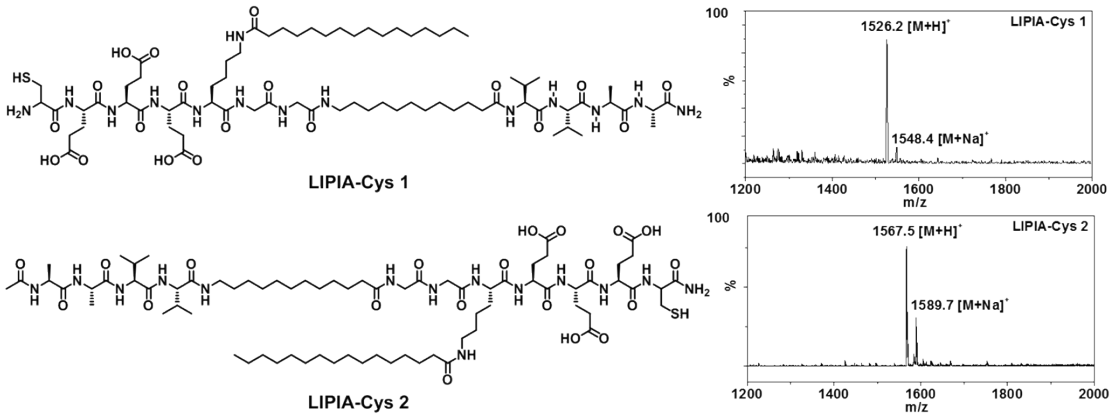

Figure S25. Chemical structures and MS spectra of LIPIA-Cys **1** s and LIPIA-Cys **2**.

6. Catalytic Experiments

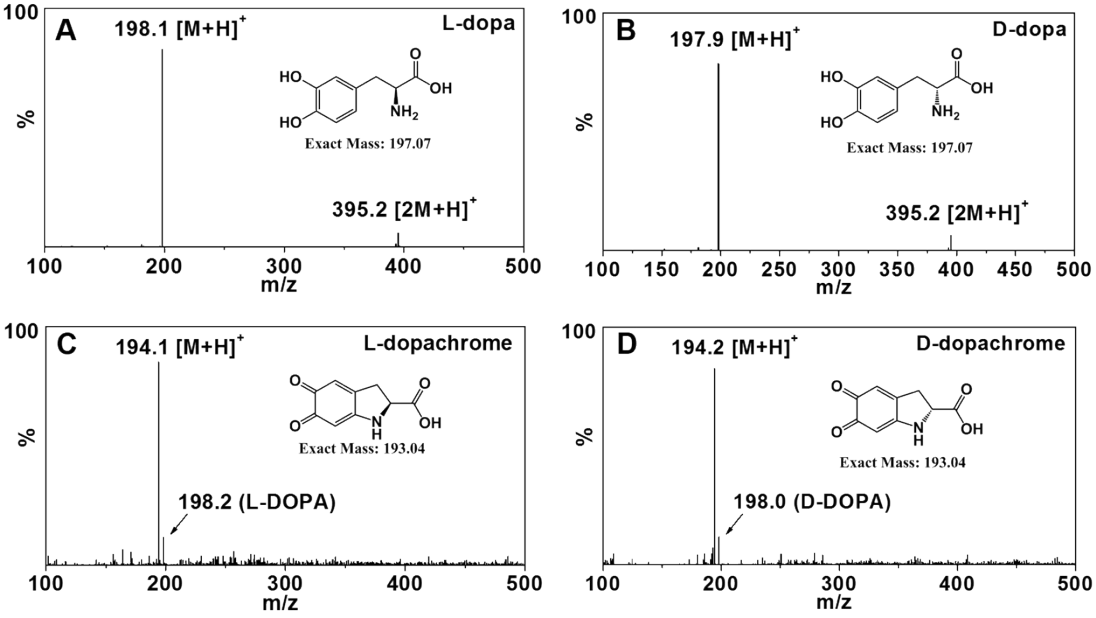

Figure S26. Chemical structures and MS spectra of L-DOPA (A) and D-DOPA (B), as well as the oxidized product L-dopachrome (C) and D-dopachrome (D) catalyzed by supramolecular nanozymes.

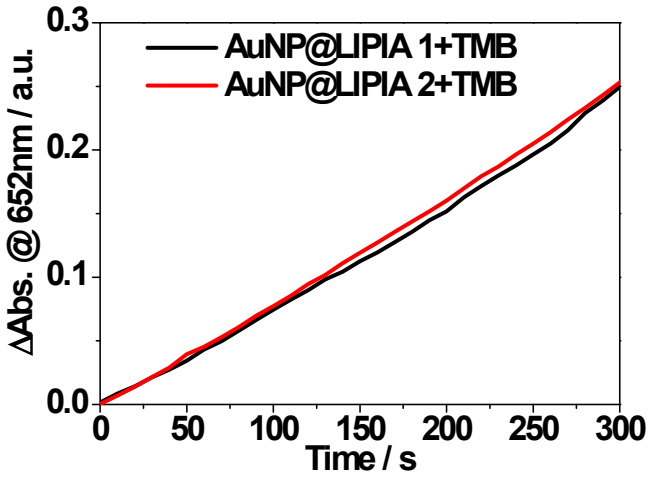

Figure S27. The changes of the UV / vis absorption intensity (@ 652 nm) of the oxidation of TMB (800 μM) as a function of time within the initial period, using either AuNP@LIPIA **1** or AuNP@LIPIA **2** as peroxidase mimics in the presence of H_2O_2 under the neutral pH condition at 25 °C.

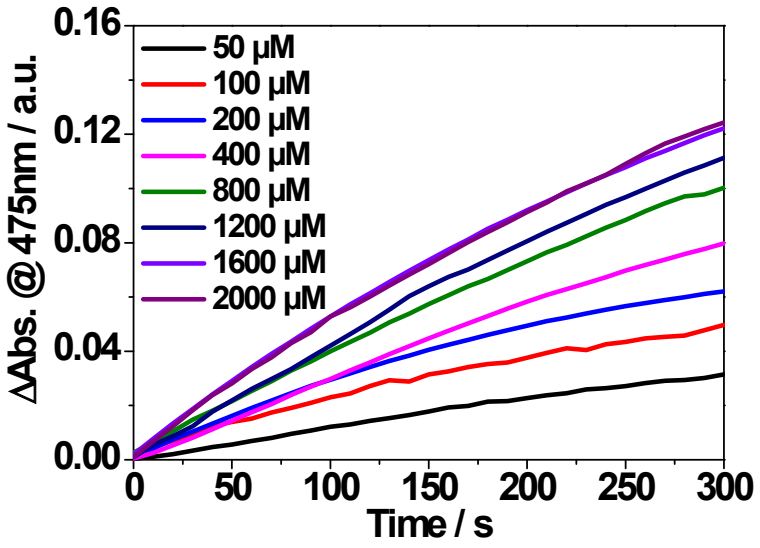

Figure S28. The changes of the UV / vis absorption intensity (@ 475 nm) of the oxidation of L-DOPA as a function of time within the initial period, using AuNP@LIPIA **1** as peroxidase mimics in the presence of H_2O_2 under the neutral pH condition at 25 °C.

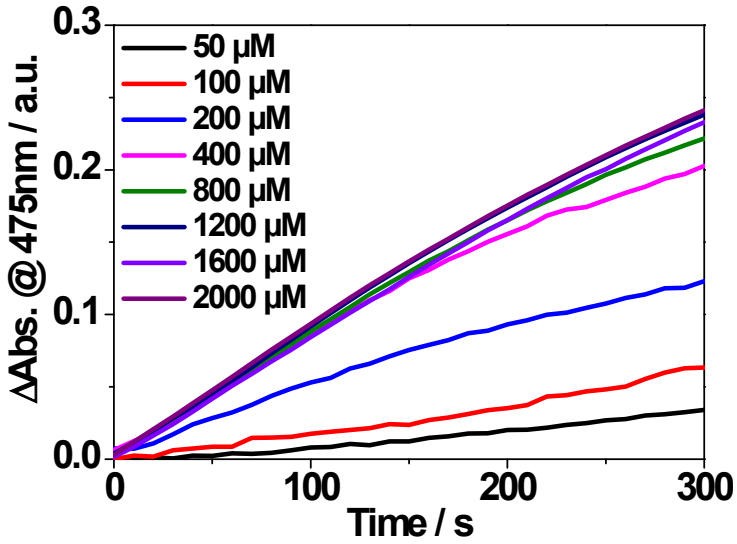

Figure S29. The changes of the UV / vis absorption intensity (@ 475 nm) of the oxidation of D-DOPA as a function of time within the initial period, using AuNP@LIPIA **1** as peroxidase mimics in the presence of H_2O_2 under the neutral pH condition at 25 °C.

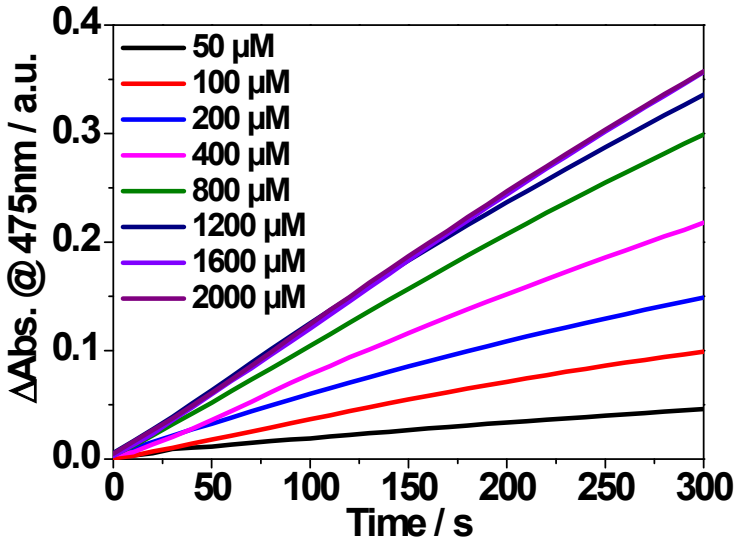

Figure S30. The changes of the UV / vis absorption intensity (@ 475 nm) of the oxidation of L-DOPA as a function of time within the initial period, using AuNP@LIPIA **2** as peroxidase mimics in the presence of H_2O_2 under the neutral pH condition at 25 °C.

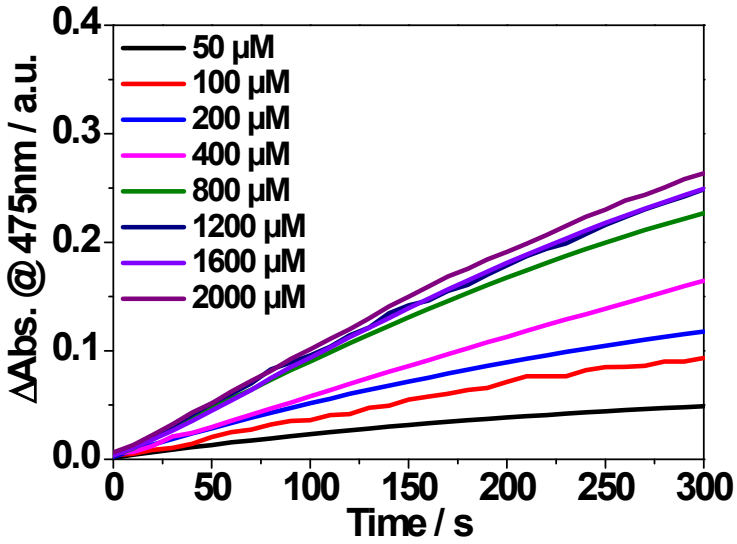

Figure S31. The changes of the UV / vis absorption intensity (@ 475 nm) of the oxidation of D-DOPA as a function of time within the initial period, using AuNP@LIPIA **2** as peroxidase mimics in the presence of H_2O_2 under the neutral pH condition at 25 °C.

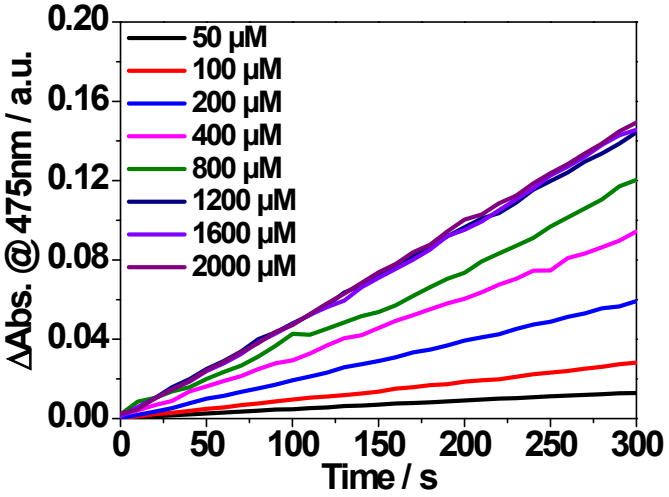

Figure S32. The changes of the UV / vis absorption intensity (@ 475 nm) of the oxidation of L-DOPA as a function of time within the initial period, using AuNPs as peroxidase mimics in the presence of H_2O_2 under the neutral pH condition at 25 °C.

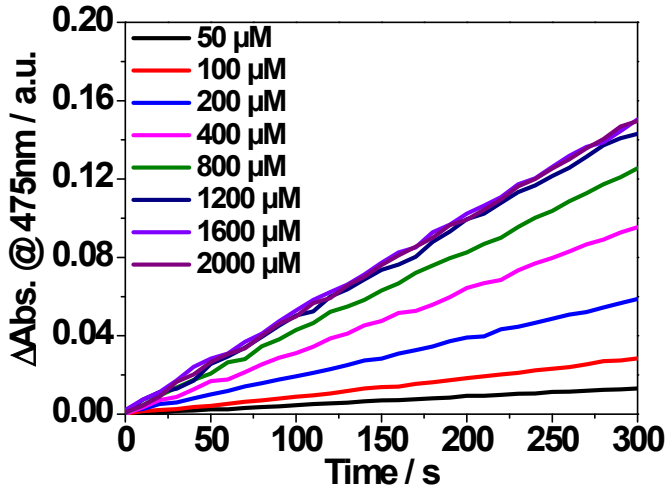

Figure S33. The changes of the UV / vis absorption intensity (@ 475 nm) of the oxidation of D-DOPA as a function of time within the initial period, using AuNPs as peroxidase mimics in the presence of H_2O_2 under the neutral pH condition at 25 °C.

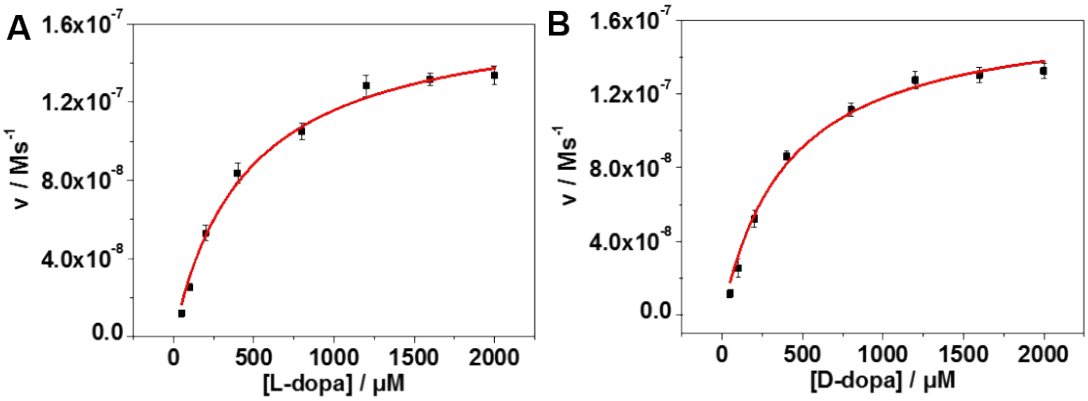

Figure S34. The initial rates of the oxidation of L-DOPA (A) and D-DOPA (B) catalyzed by AuNPs as a function of the concentration of the substrate.

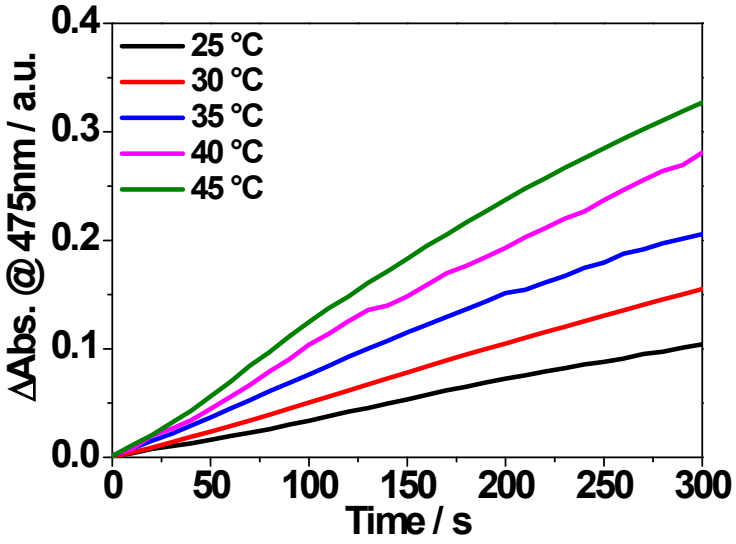

Figure S35. The changes of the UV / vis absorption intensity (@ 475 nm) of the oxidation of L-DOPA (800 μM) as a function of time within the initial period, using AuNP@LIPIA **1** as peroxidase mimics in the presence of H_2O_2 under the neutral pH condition at different temperatures.

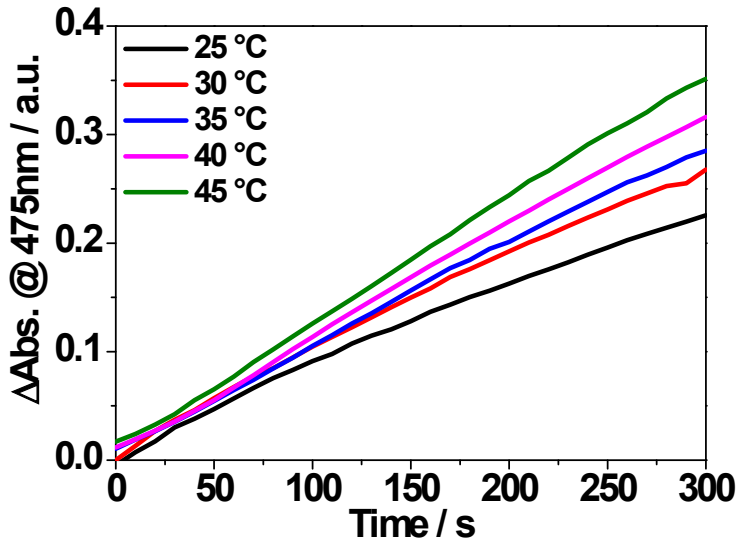

Figure S36. The changes of the UV / vis absorption intensity (@ 475 nm) of the oxidation of D-DOPA (800 μM) as a function of time within the initial period, using AuNP@LIPIA **1** as peroxidase mimics in the presence of H_2O_2 under the neutral pH condition at different temperatures.

Reference

1. M. C. Stuart, J. C. van de Pas and J. B. Engberts, *J. Phys. Org. Chem.*, 2005, **18**, 929-934.